DESIGN AND TECHNIQUE OF APERTURE FOR NEUTRON PENUMBRAL IMAGING OF Z-PINCH DIAGNOSIS PROCESS

Xiufeng WENG[1], Huasi HU[2], Tiankui ZHANG[2], Dongwei HEI[1], Mengtong QIU[1]

[1]*Northwest Institute of Nuclear Technology, NINT, Xi'an 710024, Shaanxi, China*
[2]*School of Nuclear Science & Technology, Xi'an Jiaotong University, XJTU, Xi'an 710049, Shaanxi, China*

Abstract—Penumbral coded-aperture imaging of neutrons is used to determine the spatial extent of fusion reactions in the imploded core of inertial-confinement-fusion (ICF) targets. The coded-aperture is a key to determine the image quality in the nuclear diagnosis process. The work presented in this paper focuses on forming a general method of the design and craft of the thick apertures for z-pinch diagnosis process. A special aperture, produced by D. Ress in 1990, tapered in which the radius of curvature varies inversely with distance from the source plane was regained with numerical methods. And the technique of pinhole adopting polyester-tungsten compound material instead of tungsten was established. From our experiments, apertures suited for Z-Pinch diagnosis process was successfully made out. Properties of the made-out aperture tested by Monte Carlo simulation and imaging experiments indicate that the spatial resolution of the aperture reaches 250 μm over a field of view of 1 cm. The achievements are of reference value to the experimental study of prompt radiation imaging diagnosis in the near future.

Keywords—Penumbral imaging, Isoplanaticity, Z-Pinch, Spatial Resolution, Technique

I. INTRODUCTION

In inertial confinement fusion (ICF), when fusion happens, the target center is in the extreme temperature and pressure state, and large numbers of alpha particle, proton and neutron, γ-rays and x-rays leak out [14, 15]. Detecting these leaked radiations can provide useful information on symmetry, uniformity, hydrodynamic instability, even absolute intensity and intensity distribution changes over time of the fusion source region.

Compared with x-rays from the target capsule plasma, however, neutrons and charged particles are the direct products of nuclear fusion. Accordingly, imaging of neutrons and charged particles can provide more direct information about the size and symmetry of the fusion core. Comparatively, neutrons can bring out better information about the spatial scale, shape, and uniformity of the implosion compression area of the fusion target capsule. So, neutron imaging has been widely developed in fusion diagnosis since 1980s of the last century.

In order to obtain high quality image of 14 MeV neutrons from thermonuclear fusion, it is demanded that reaction efficiency of detecting materials or neutron yield should be high enough. However, limited by the existing materials' detection efficiency to 14 MeV neutrons as well as the neutron yield of present fusion devices (generally less than 10^{13} neutrons), the direct image measurement based on neutron pinhole imaging becomes hard to use, which urged the development of indirect method using neutron penumbral imaging technique.

Neutron penumbral imaging, when used in diagnosis of low-neutron-yield fusion process, has the following advantages compared with the neutron pinhole imaging: Firstly, process with low-yield neutrons [10] can be diagnosed while the latter can often be used in detection of reactions releasing high-intensity neutrons; secondly, the spatial resolution of the source area is higher than the latter one; thirdly, in neutron penumbral imaging, the aperture can be

larger than the fusion source, which let the difficulty of apertures' machining dramatically reduced.

However, penumbral images are complex encoded images; a great deal of decoding calculation is needed in image reconstruction. In recent years with the rapid development of computer technology, the lower computer costs and the faster computing speed, the excellent computer data-processing capability make real-time response to nuclear reaction imaging possible. So neutron penumbral imaging has become one of the effective diagnostic means to ICF.

The results on neutron penumbral imaging at the Nova laser fusion device in Livermore Laboratory (LLNL) was reported by D. Ress et al. [2]. The feasibility of 14 MeV fusion neutron imaging was proved. Subsequently Dsieder et al. [5–6, 11–13] also did some studies on neutron penumbral imaging at OMEGA laser device in the United States. Chen et al. [9, 10] made a lot of researches on SG-II fusion facility using neutron penumbral imaging in China.

In 1990, D. Ress proposed a method of designing the penumbral aperture [7], and applied it into Nova laser fusion experiment, achieving 10 μm spatial resolution [2, 7]. However, the technique of the penumbral aperture seems too demanding in terms with the present manufacturing techniques.

In this paper, we hope to bypass the limit of manufacturing and propose an economical technique of making the penumbral aperture for Z-pinch diagnosis process. In our study, the model of neutron pinhole penumbral imaging system was firstly built and simulated with MCNP program; then, the apertures suitable for Z-pinch process was designed out on basis of the methods advocated by D. Ress [7]. Thirdly, the techniques of aperture adopting polyester-tungsten compound material [8] instead of tungsten and gold were established. A set of procedures were gained by about two-year trials and experiments and the apertures with a theoretical spatial resolution of 250 μm over a field view of 1 cm was trial-produced.

II. DESIGN OF PENUMBRAL APERTURE

Dress has advocated a novel method to design the neutron penumbral aperture for Nova in 1990 [7]. According to his idea, high-resolution penumbral imaging of weak sources of penetrating radiation requires an aperture with the following set of characteristics. First, adequate contrast requires use of an aperture several mean free paths thick. The resulting aperture must often be many centimeters thick. Next, the aperture point-spread function (PSF) must have a sufficiently sharp cutoff. In addition, to obtain an image of a relatively weak source with an acceptable signal-to-noise ratio requires that the aperture be quite close to the source. Finally, penumbral imaging requires numerical reconstruction of a coded image to obtain an estimate of the source. The computational difficulty of the reconstruction is vastly reduced through use of an isoplanatic aperture and linear reconstruction techniques. Therefore, imaging system magnification must be reasonably uniform across a useful field of view.

A simple analytic approach to aperture meeting these conditions is a taper in which the radius of curvature varies inversely with distance from the source plane, which is called an IRC aperture. The PSF of the designed aperture is sufficiently isoplanatic and distortion free to allow the use of fast linear reconstruction methods in unfolding the coded images.

The cutoff of PSF of the penumbral aperture determines the spatial resolution. One way to make the aperture isoplanatic is requiring that the aperture cutoffs corresponding to different points in the field of view be as similar as possible.

In Figure 1, consider the intersection of a ray with a circle of radius R centered at the origin of the coordinate system; the ray leaves the source at angle θ. To determine the length Δz of the chord intercepted by the ray we locate the intersection points, which are determined

by the equations

$$\begin{cases} \rho - R = \theta(z - z_i) \\ \rho^2 + z^2 = R^2 \end{cases} \tag{1}$$

where z_i is the distance between the source and the aperture at the point of first intersection (tangency).

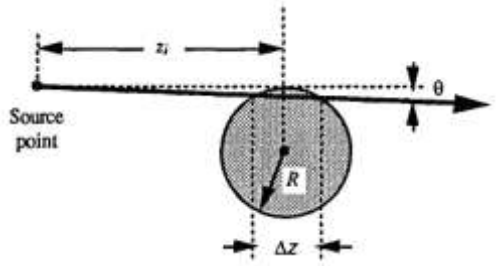

Figure 1. A ray from a source point cuts a circle of radius R (cited from Figure 1 of [10]).

The path length through the circle can be formulated as follows

$$\Delta z = 2\sqrt{R^2 - [(R - \theta z_i)\cos\theta]^2}$$
$$= 2R\sqrt{1 - [(1 - \frac{\theta z_i}{R})\cos\theta]^2} \quad .$$

Do Taylor expand to $\cos\theta$, $\cos^2\theta = 1 - 2\cdot\frac{\theta^2}{2} + \frac{\theta^4}{4} \cong 1 - \theta^2$. Let's denote $q = \frac{\theta z_i}{R}$, then, we have

$$\Delta z = 2R\sqrt{1 - (1-q)^2(1-\theta^2)} = 2R(1-q)\sqrt{\frac{1}{(1-q)^2} - 1 + \theta^2}, \tag{2}$$

where it is assumed that $\theta << 1$, $z_i / R << 1$ and $q << 1$. Thus, we have

$$\Delta z = 2R\sqrt{\theta^2 + 2q} \ .$$

With the restriction of $\Delta z << z_m$ (z_m – the mean free path within the aperture material), the first term under the radical can be neglected, so we have

$$\Delta z = 2\sqrt{2Rz_i\theta}$$

and it is now clear that Δz will be approximately independent if R varies as $1/z_i$.

Now take R as the (variable) radius of curvature of a tapered cylindrical aperture. Rays from different source points in the field of view will intersect the aperture with different values of z_i. If R_0 is the radius of curvature at the front face of the aperture, and if that face is separated from the source by a distance z_0, we have

$$R = \frac{z_0}{z} R \ ;$$

replacing $1/R$ with the usual expression for the curvature, we obtain a second-order, nonlinear, ordinary differential equation

$$\frac{d^2\rho}{dz^2} = \frac{z}{z_0 R_0}[1 + (\frac{d\rho}{dz})^2]^{3/2} \tag{3}$$

It is desirable to specify the aperture in terms of its initial diameter, the source-plane-to-aperture-entrance separation z_0, the aperture thickness z_t , and the field-of-view diameter d_{fov} .

For ICF process driven by Z-pinch, the field view of the source area is typically as big as 1cm. The setup and key parameters of the detection system are as followings: the magnification of

the imaging system is fivefold, source-plane-to-aperture-entrance separation $z_0 = 24\ cm$, the aperture thickness $z_t = 6\ cm$, the diameter of the end of aperture subtending to the source 5mm with the counterpart 6 mm. The schematic is shown in Figure 2.

With these initial conditions, to solve the equation (3), employing Mathematica software, discrete data of the outlines of the aperture, i.e. taper function, along z-axis are acquired, displayed in Figure 3. The 600 set of data is fragmented into 20 fractions. The deviation between the fractioned and the theoretical taper function is controlled in 1 μm.

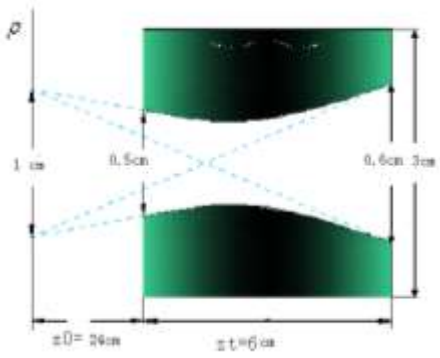

Figure 2. Schematic of design of IRC aperture for z-pinch process.

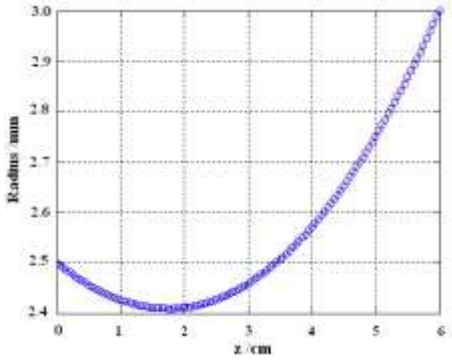

Figure 3. Taper function of designed aperture for z-pinch process.

In the next step, the outer radius of the coded aperture should be determined. The point spread function of 5 cm × 5 cm optic fiber system with different outer radius was calculated. The best appropriate radius should have the largest dynamic range. Take R = 0.8, 1.0, 1.5, 2.0, 5.0 to do calculation respectively.

As indicated in Figure 4, the penumbral aperture cannot effectively shield rays projecting from the source once the outer radius ≤1 cm, which hints us that the radius should be larger than 1 cm. However, given the increased scattering rays, which will deteriorate the dynamic range of the optic fiber scintillation array, caused by more quantity of shielding materials, we narrowed the scope of radius to 1.1~1.5 cm. The PSF of the energy deposition is shown in the following figure.

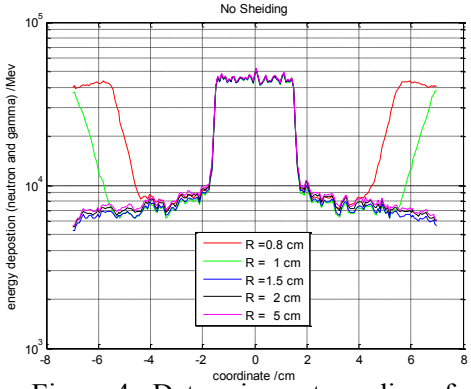

Figure 4. Determine outer radius of coded aperture initially.

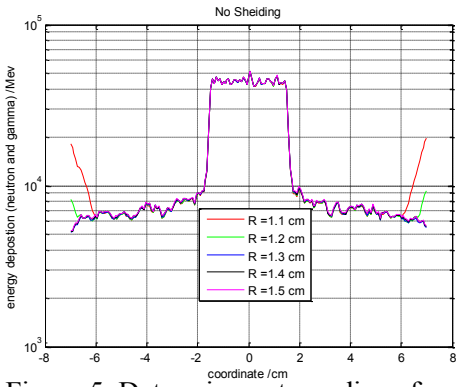

Figure 5. Determine outer radius of aperture.

From Figure 5, we can conclude that PSF of radius 1.3 ~ 1.5 cm has the best dynamic range. In the paper, the outer radius of the coded aperture is determined as 1.5 cm. The schematic of the designed penumbral coded aperture has been shown in Figure 2.

III. PROPERTIES OF DESIGNED PENUMBRAL APERTURE

Properties such as the isoplanaticity, dynamic range and spatial resolution etc. of the designed penumbral aperture were calculated using Monte Carlo method.

A. Isoplanaticity

In order to test the isoplanaticity of the aperture, a series of source position with varied offset should be taken into account when simulating.

Some distance of offsets, herby from -0.5cm to 0.5cm, between the point source and the axis origin, were plotted and each corresponding point spread function was calculated for comparison, as shown in Figure 6. After moved to the axis center in the distance of the corresponding offset, the PSF image in Figure 6 became almost the same shown in Figure 7. It can be concluded that PSF of every point in the source plane are isoplanatic, i.e. axial symmetry.

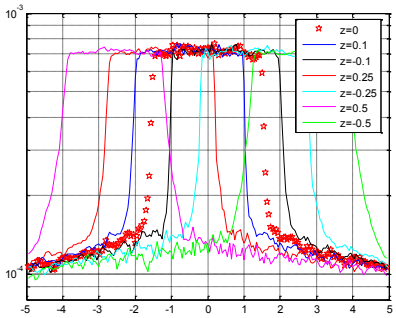

Figure 6. PSF with the point source offset axis.

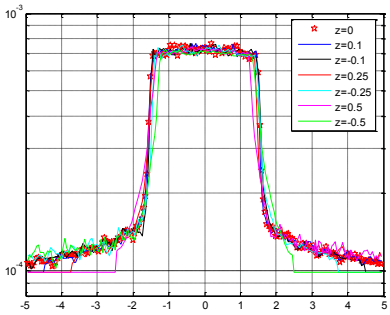

Figure 7. PSF after moving to the axis center.

Point spread function of neutron penumbral imaging system with a large source view of 1cm and magnitude 5 suited for diagnosis of Z-Pinch physical process is sketched in Figure 8.

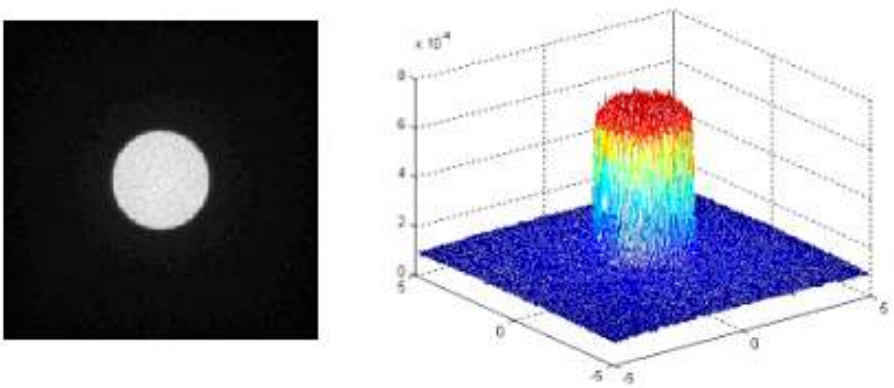

Figure 8. PSF of neutron penumbral imaging system with large view for diagnosis of z-pinch process. Left: PSF shown in grey scale. Right: PSF shown in 3-D graphics.

Point space on the source plane is set between 200 μm and 500 μm. Iterating 3000 generations of PSF sketched in Figure 8 by Richardson-Lucy algorithm, which is based on Bayesian statistics nonlinear iteration, we get a series of results sketched in Figure 9.

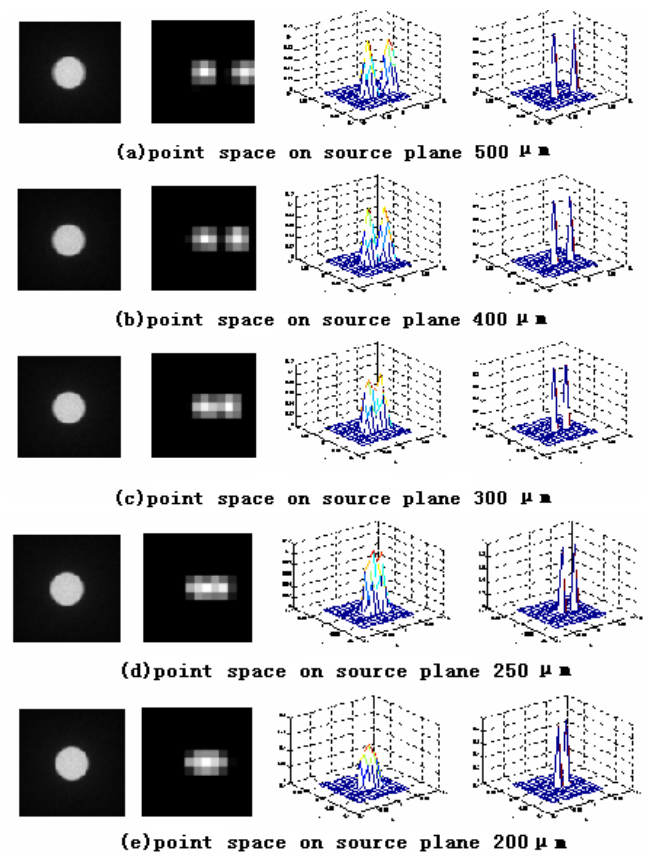

Figure 9. Test of the spatial resolution of the source plane.

Figure 9 indicates that when point space on source plane gets close to 250 μm, the summit of the two neighborhood point can just be exactly discriminated. Therefore, the spatial resolution of the designed penumbral aperture for large view diagnosis of z-pinch process is 250 μm. Compared the absolute value with the resolution 10 μm gained in ICF driven by laser beam [7], the spatial resolution 250 μm is inferior to that of the latter one. However, to compare the relative spatial resolution, in z-pinch process, 250 μm is obtained over 1cm field of view, while in IRC driven by laser beam, 10 μm is attained over the 150 μm field of view. The relativity of the resolution over the field of view is 0.025 and 0.066, respectively.

IV. TECHNIQUE OF PENUMBRAL APERTURE

Technique of penumbral aperture driven by laser beam has been in-depth researched [2,7]. As to the technique of penumbral aperture suited for Z-pinch driven diagnosis, Prof. HU Huasi [8] proposed a method of fast and once formation, adopting polymer-tungsten compound materials.

Prof. HU Huasi's group has researched shielding properties of polymer-tungsten composite material [8] in the past years. Bisphenol A epoxy resin E-51 and polyamide 650 are employed as matrices of compound materials. When the bisphenol A and polyamide are mixed together, it is too sticky to be mixed well without using some diluents. So, acetone is used as diluents to improve the fluidity. The mass ratio of tungsten to polymers is 95% to 5%, of which 5% the ratio of bisphenol A to polyamide 650 is 100:60. Almost all the acetone can be volatilized over the solidification course, so the quantity of acetone put into the compound materials can be added on empirical experiments.

A. Fabrication of mold

The mold for once-formation of compound materials consists of outer cylinder cladding and the central “needle stick”. The “needle stick” is fixed in the center of the mold over the forming process. The mixture of the compound materials are stuffed into the gap. Once the solidification course is over, disassemble the mold and the “needle stick”.

When designing the mold, the following factors should be taken into account: firstly, the size of the mold should keep consistent with designed penumbral coded aperture; secondly, the structure should be convenient for disassembly; thirdly, there should be some air holes for release of volatilized acetone and for leakage of compound materials when they are under heavy pressure.

The choice of the mold material was done through experiments. Initially, we make the mold with steel 45#, but it turned out that after solidification the outer mold cladding and the in-between compound materials get tighter and cannot be separated, which is suspected owing to the small thermal heat conductivity gap between the 45# steel and the compound materials. Afterwards, the aluminum, with better heat conductivity than steel, was tried as the mold material, consequently it made separating the mold from compound materials much easier. Moreover, the mold is carved into half. Over solidification course, two steel hoops are used to tighten the two halves together and after solidification, the hoops get loose for convenience of separating the two halves.

The fabrication of the mold can be made with simple machining technology. Through multi trial-designs and improvements, the final mold is designed and fabricated as Figure 10.

Figure 10. The mold for once-formation of compound materials.

Regarding the “needle stick”, it is the core component for fabricating the penumbral aperture. The designed aperture can be obtained after separating the “needle stick” from the mold cladding and the compound materials. The outline of the arc in the middle of the “needle stick” strictly agrees with the designed taper function. On the basis of the discrete data gained in part Ⅱ, the “needle stick” can be produced via high-precision digital control machine. The schematic for manufacturing of the needle mold is sketched in Figure 11.

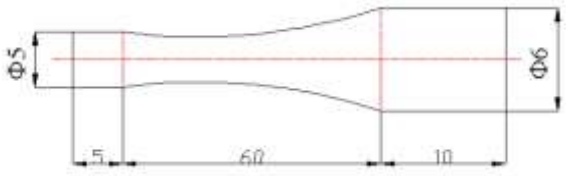

Figure 11. Schematic for manufacturing of the needle mandrel.

In Shaangu Xiyi Group Co., limited, the needle made of steel 45 is manufactured. The six hundred discrete data of the taper function given are divided into fractions with each 5 set

of data, program them into the digital control machine, and then the “needle stick” was made out.

B. Trial-produce of the penumbral aperture

Materials such as bisphenol A resin E-51, polyamide 650 and tungsten and titanium dioxide, and the instruments such as vacuum evacuation machine, incubator, mixer, screw jack and mould are used in our trial-produce experiments, shown in Figure 12 and Figure 13, respectively.

Figure 12. Materials for experiments. Left: bisphenol A resin E-51. Middle: polyamide 650. Right: tungsten and titanium dioxide.

Figure 13. Instruments for experiments. From left to right: vacuum evacuation machine; incubator; mixer; screw jack and mold.

The technique flowchart is as follows:

(1) Design the mold and produce.
(2) Design the needle mandrel and produce.
(3) Smear silicon oil on the inner surface of the mold and the outer surface of the “needle stick”
(4) In terms with the ratio of the materials, weigh tungsten 950g, bisphenol A 32g, polyamide 18g, titanium dioxide 1.5g.
(5) Add about 100mL acetone as dilution; mix the materials sufficiently and uniformly with the mixer.
(6) Put the well-mixed polymer-tungsten in the vacuum evacuation machine, pump air and acetone. Repeat pumping 2-3 times.
(7) Pressurize the compound materials with the screw jack. Put them wholly into the incubator to solidify.
(8) The solidification course is set on the program that the materials are bathed under 50℃ for three hours, then one hour under 70℃ and the last two hours under 130℃.
(9) Separate mold.
(10) Corrode the smaller radius end of the “needle stick” with nitrate of volume concentration 50%.

(11) Remove the mold from the aperture and clean the aperture.

Some notices should be paid attention to. Firstly, the carbon steel is selected as material of the “needle stick” instead of the stainless steel, which is mainly because that stainless steel cannot be corroded by acids. Secondly, the end cap of the mold is perforated and a layer of copper gauze on the inner surface of the cap is coved. The air in the compound materials can get released through the hole, meanwhile the compound materials will not overflow when pressurizing. Thirdly, the quantity of acetone should be added little by little, which depends on the status of the compound materials. Once acetone is added more without sufficient pumping in vacuum pump, air holes may accumulate in the materials, which will deteriorate the shielding of the materials. Once not enough, it will be hard to get materials mixed uniformly. Compared with the excess of acetone, the "not enough" cannot make the materials mix well. Over use of acetone will not that matter if the air inner the materials is pumped sufficiently. Figure 14 is one common phenomenon that air of materials is not evacuated well with much acetone. Through experiments, we figure out that an empiric quantity of acetone is around 100mL. Fourthly, pump air at least twice. The first time of pumping air from the materials in the mold can be done without loading force upon the materials; in the second or third time, press the materials hardly with a screw jack; at the last time, push them mildly till the length of the aperture meet the needs. When air inner the materials is exhausted, put the whole instrument into the incubator. Over the process, if heavily compressed, the compound materials will rupture, as shown in Figure 15. Fifthly, in the process of acid corrosion of the “needle stick”, when we compound nitric acid solution with volume concentration 50% for use, the hot water should be used. By experiments, it is found that nitric acid solution compounded by water of room temperature cannot make the etching react. When we change water with room temperature to 100℃ water, the corrosion reaction reacts quickly and for just a several minutes the mandrel is etched to the extent that it can be removed from the solidified compound materials. Sixthly, separate the mold immediately the solidification course in the incubator is over. It is not easy to separate the materials from the mold and the “needle stick” when materials cool down in the air. Once cooled down, reheat them in the incubator for about 20 minutes first, and then do the separation.

The points above are all summarized from about two-year experiments. The penumbral aperture for diagnosis of z-pinch process trial-produced is demonstrated in Figure 16.

Figure 14. Air holes in materials.

Figure 15. Over load on materials.

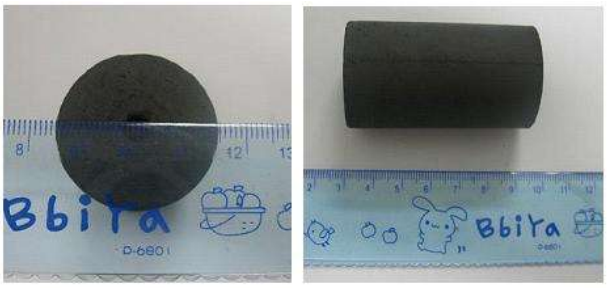

Figure 16. Trial-produced IRC aperture for z-pinch diagnosis process.

The trial-produced penumbral aperture in Figure16 has 3 cm outer radius, 6 cm thickness, and consistent inner outlines designed and shown in Figure 3.

V. SUMMARY

The designing method of thick aperture for high-resolution penumbral imaging put forward by D. Ress is applied in designing the penumbral coded aperture for diagnosis of z-pinch process with large field of view. The properties of designed penumbral aperture for z-pinch diagnosis are calculated by MCNP simulation. The designed aperture has about a spatial resolution of 250 μm over a 1 cm field of view.

The once formation technique with polymer-tungsten composite materials was established by trials and experiments. A fabrication process was finally formed. We can fulfill the fabrication of the aperture by employing only the common machining technology and common operation process. So the cost of producing apertures suited for the system was greatly lowered down. The research provides a reference for fabricating collimators or apertures of the neutron penumbral imaging system in diagnosis of z-pinch physical process. However, there still exist some limits in our technique. In our experiments, forces of screw jack on materials are loaded based on empirical trials. Maybe more quantitative studies on the technique will turn out a better result. Further study of imaging experiments with the aperture also needs to be taken into account.

ACKNOWLEDGMENT

The work is performed under the auspices of the National Natural Science Fundation of China under the contract number 10576022 and the National Universities Students Innovation Experimental Project of Minister of Education of the P.R.C under the contract number 610709.

The authors are appreciated for discussion with professor Quncheng Fan in the school of Mechnical Engineering of Xi'an Jiaotong University. The author also would like to thank master worker in machining Yuyin Liu.

REFERENCES

1. Nugent K.A., Luther D.B. Penumbral imaging of high energy X-rays from laser-produced plasmas. Opt. Commun., 1984, 49: 393－401.
2. Ress D., Lerche R.A., Eill R.J., et al. Neutron imaging of laser-fusion targets. Science, 1988, 241: 956－960.

3. Mosinski G., Roy B. CEA Bruyeres le Chatel, Diagnostic Development at LLNL for National Ignition Facility. Report No. 79/DR 83. Livermore: Department of Energy's National Nuclear Security Administration in the US, 1983, 1－4.
4. Sommargren G.E., Lerche R.A. Neutron Imaging of ICF Target plasmas. Report No. CA, UCID-19317. Livermore: Lawrence Livermore National Laboratory, 1988, 1－5.
5. Disdier L., Rouyer A., Wilson D.C., et al. High-resolution neutron imaging of laser imploded DT targets. Nucl. Instrum . Meth. A, 2002, 496:502－506.
6. Chen Y.W., Otsuki K., Nakao Z. Blind reconstruction of X-ray penumbral images. Rev. Sci. Instrum., 1998, 69(5): 1966－1969.
7. Ress D. Neutron imaging for inertial-confinement-fusion experiment. IEEE Trans. Nucl. Sci., 1996, 37(2): 155－160.
8. Hu H.S., Wang Q.S., Juan Q., et al. Study on composite material for shielding mixed neutron and γ -rays. IEEE Trans. Nucl. Sci., 2008, 55(4):2376－2382.
9. Liu D.J., Tang X.H., Zhao Z.Q., et al. Neutron imaging penumbral image inversion method (in Chinese). Laser and particle beams, 2006, 18(7): 1199－1202.
10. Fa-Xin Chen, Zheng, Jian-Lun Yang. Thick neutron pinhole imaging numerical simulation (in Chinese). Acta Phys. Sin., 2006, 55(11): 5947－5952.
11. Nugent K.A. Coded imaging of thermonuclear neutron. Rev. Sci. Instrum., 1988, 59(8): 1658－1659.
12. Rouyer A. Rev. Sci. Instrum., 2003, 74(3): 1234－1236.
13. Disier L., Rouyer A., Wilson D.C., et al. High-resolution neutron imaging of laser imploded DT targets. Nucl. Instrum. Meth. Phys. Res. A, 2002, 489(123): 496－502.